ACS OMEGA

http://pubs.acs.org/journal/acsodf

Article

Determining the Thermal Properties of Buckypapers Used in Photothermal Desorption

Jacob S. Shedd, Wyatt W. Kuehster, Smriti Ranjit, Adam J. Hauser, Evan L. Floyd, Jonghwa Oh, and Claudiu T. Lungu*

Cite This: *ACS Omega* 2021, 6, 5415−5422

Read Online

ACCESS | Metrics & More | Article Recommendations | Supporting Information

ABSTRACT: Volatile organic compounds (VOCs) pose an occupational exposure risk due to their commonplace usage across industrial and vocational sectors. With millions of workers annually exposed, monitoring personal VOC exposures becomes an important task. As such, there is a need to improve current monitoring techniques by increasing sensitivity and reducing analysis costs. Recently, our lab developed a novel, preanalytical technique known as photothermal desorption (PTD). PTD uses pulses of high-energy, visible light to thermally desorb analytes from carbonaceous sorbents, with single-walled carbon nanotube buckypapers (BPs) having the best overall performance. To apply this new technology most effectively for chemical analysis, a better understanding of the theoretical framework of the thermal phenomena behind PTD must be gained. The objectives of the present work were 3-fold: measure the thermal response of BPs during irradiation with light; determine the best method for conducting such measurements; and determine the thermal conductivity of BPs. BPs were exposed to four energy densities, produced by light pulses, ranging from 0.28 to 1.33 J/cm^2, produced by a xenon flash lamp. The resulting temperature measurements were obtained via fast response thermocouple (T/C) mounted to BPs by three techniques (pressing, adhering, and embedding). Temperature increase measured by T/C using the adhering and pressing techniques resulted in similar values, 29.2 ± 0.8 to 56 ± 3 °C and 29.1 ± 0.9 to 50 ± 5 °C, respectively, while temperature increase measured by embedding the T/C into the BP showed statistically larger increases ranging from 35.2 ± 0.9 to 76 ± 4 °C. Peak BP temperatures for each mounting technique were also compared with the temperatures generated by the light source, which resulted in embedded BPs demonstrating the most temperature conversion among the techniques (74−86%). Based on these results, embedding T/Cs into the BP was concluded to be the best way to measure BP thermal response during PTD. Additionally, the present work modeled BP thermal conductivity using a steady-state comparative technique and found the material's conductivity to be 10.6 ± 0.6 W/m^2. The present work's findings will help pave the way for future developments of the PTD method by allowing calculation of the energy density necessary to attain a desired sorbent temperature and providing a means for comparing BP fabrication techniques and evaluating BP suitability for PTD before conducting PTD trials with analytes of interest. Sorbents with greater thermal conductivity are expected to desorb more evenly and withstand higher energy density exposures.

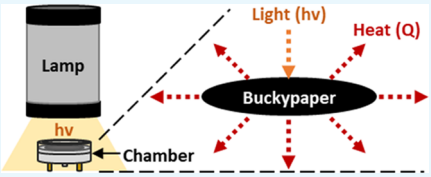

1. INTRODUCTION

Volatile organic compounds (VOCs) are ubiquitously used across multiple industrial and vocational sectors, with some VOCs being capable of creating health hazards. According to the United States Bureau of Labor Statistics,[1] millions of employees work in occupations known to use VOC-containing products, indicating a high potential for worker exposure to VOCs. Over the years, many validated methods have been developed to quantify occupational exposures[2−4] to VOCs for compliance with occupational safety and health regulations and comparison with occupational exposure limits (OELs) set by governmental[5] and professional regulatory bodies.[6,7] These methods traditionally required sample collection to be conducted using a pump with an in-line sorbent tube, but in recent years, diffusive samplers have become a desirable alternative due to their small, lightweight design and simple operation, which does not require pumps, tubing, and field calibration. Despite their advantages, diffusive samplers have sensitivity limitations due to their low mass uptake rate (diffusion driven), making them less desirable in sampling for short durations and/or low analyte concentrations. This could be an issue when highly toxic chemicals are present in low concentrations. Sensitivity is further limited by current analysis techniques such as the National Institute of Occupational Safety and Health's (NIOSH) analytical methods 1500[2] and 1501[3] that employ chemical desorption (CD) with CS_2 to extract analytes from the sample medium, effectively diluting the sample. The methods then specify injection of a 1 μL aliquot of the desorbed solution into a gas chromatograph,

Received: November 17, 2020
Accepted: February 3, 2021
Published: February 17, 2021

https://dx.doi.org/10.1021/acsomega.0c05613
ACS Omega 2021, 6, 5415−5422

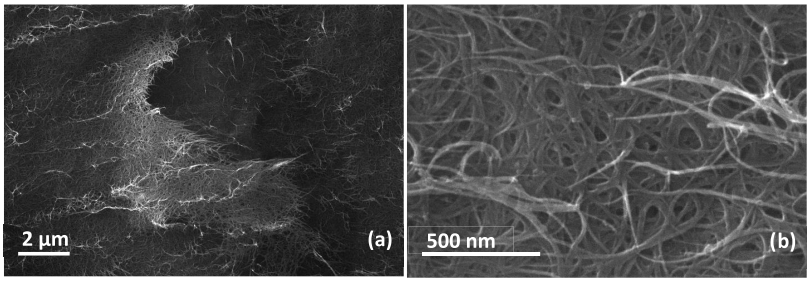

Figure 1. SEM images of an AD BP at magnifications at 14 100× (a) and 161 000× (b).

resulting in only 0.1% of the diluted analyte mass being used for analysis. By making improvements to the methods of analyte desorption and delivery to instrumentation, the sensitivity of diffusive samplers could be increased. This would make diffusive samplers suitable for a wider array of sampling scenarios, such as low concentration and short-term air sampling. These improvements would also reduce labor and cost associated with laboratory analysis.

In response to the limitations of current methodologies, our lab recently developed a preanalysis technique referred to as photothermal desorption (PTD). PTD uses pulses of high-energy, visible light to desorb volatile compounds from dosed sorbents,[8,9] eliminating the need for sample extraction and dilution as preanalysis work-ups. PTD's novel approach to desorption allows for repeat desorption[8] of samples and up to 0.4% mass recovery per desorption cycle (i.e., flash),[9] which means PTD is capable of delivering a sample mass 4 times greater than that produced by CD. To do so, PTD utilizes the thermal and adsorptive properties of single-walled carbon nanotubes (SWNTs) to capture and release analytes for eventual analysis. Using PTD, successful desorption of toluene from carbon nanotube felts and buckypapers (BPs) has been demonstrated[8,9] by taking advantage of two characteristics of SWNTs: high thermal conductivity and efficient heat conversion of absorbed light.[10−14] Utilizing these properties, SWNT felts, i.e., SWNTs laminated onto a silver membrane filter for structural support, were demonstrated to have reproducible toluene desorption, in relation to light energy.[15] When compared to coconut shell-activated carbon, SWNT felts showed a significantly higher desorption. This effect was believed to result from the rapid distribution of heat throughout the sorbent bulk material, facilitated by the high thermal conductivity of SWNT felts.[8]

In the years since PTD was first conceptualized, durable, self-supporting BPs have been reliably produced for use with PTD using arc discharge (AD) SWNTs. The process for producing the most adsorptive BPs has been identified,[16,17] and their adsorption capacities for toluene,[16] an aromatic VOC, have been determined. However, the thermal characteristics of this material and how they contribute to the theoretical framework of PTD have yet to be empirically explored. Though various theoretical and experimental thermal conductivity values have been reported in the literature for SWNTs, BPs, and single-layer graphene,[10,11,18−21] the need to investigate the thermal response of BPs to light exposure, and the thermal conductivity of AD SWNT BPs specifically, remains.

The purpose of the present study was to determine the thermal response of BPs to visible, radiant energy input and characterize the thermal conductivity of BPs, as means of investigating and quantifying the driving forces behind the novel PTD technique (i.e., the theoretical framework). This was accomplished by achieving three main objectives: measuring the thermal response of BPs during PTD, determining the most reliable method for measuring thermal response, and quantifying the thermal conductivity of BPs. By investigating the thermal characteristics of BPs, this study has also attempted to define and explain the thermal limitations (i.e., range of achievable desorption temperatures) of PTD; this, in turn, will allow for better insight into the analytical capabilities of PTD, based on the thermal energy input required to desorb a given mass of analyte from the surface of BPs.

2. RESULTS

2.1. Morphological Analysis. The scanning electron microscope (SEM) images of a representative BP sample are shown in Figure 1. These images provide insight into the BP general morphology. At lower magnifications (14 100×; Figure 1a), it is evident that the BP surface is nonuniform due to uneven distribution of SWNT and composed of fiber bundles. At higher magnification (161 000×; Figure 1b), the BP was observed to be constructed of a highly interconnected and randomly aligned SWNT network. Discrete nanofibers were seen interwoven into large bundles, thus giving rise to micro and nanoscale pores and high surface area contact between individual fibers within the material. This interconnected structure is expected to allow good thermal conduction across layers as well as within layers due to the high axial thermal conductivity of SWNT fibers.

2.2. Thermal Response. The peak thermal response of BPs irradiated at four energy densities and measured by three T/C mounting techniques are reported in Table 1. The presented data are directly linked to the respective lamp energy densities, the distance between lamp and sample (2.9 mm), and the light exposure time (0.0005 s).[22] Multiple linear regression modeling (R-squared = 0.91) of the thermal response data showed that mean peak temperatures are

Table 1. Average, Peak Temperatures of BPs at Different Energy Densities for Three T/C Mounting Methods

energy density (J/cm^2)[a,b]	peak temperature (°C)[a,c]			
	pressed	adhered	embedded	p-value[d]
0.28 ± 0.02	29.1 ± 0.9	29.2 ± 0.8	35.2 ± 0.9	<0.0001
0.42 ± 0.01	32 ± 2	32.8 ± 0.7	41 ± 1	
0.728 ± 0.009	38 ± 3	40 ± 2	53 ± 1	
1.33 ± 0.01	50 ± 5	56 ± 3	76 ± 4	

[a]Values are depicted as mean ± standard deviation. [b]n = 30. [c]n = 9. [d]α = 0.05.

https://dx.doi.org/10.1021/acsomega.0c05613
ACS Omega 2021, 6, 5415−5422

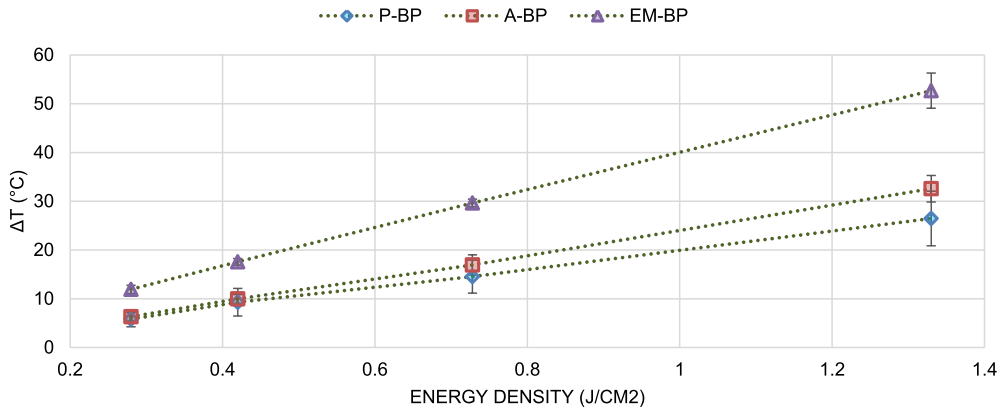

Figure 2. Peak temperature differentials (ΔT_{BP}) averaged from three replicate trails at energy density and each T/C attachment method.

statistically different across all three T/C mounting methods ($p < 0.0001$). Post hoc analysis via Tukey's test confirmed that the embedded BP recorded the highest averaged peak temperatures over all light settings among the three methods, with temperatures measuring 11.8 °C (95% confidence interval (CI) = [9.4, 14.1]) higher than the adhered BP, and 14.0 °C (95% CI = [11.7, 16.3]) higher than the pressed BP.

Average BP temperature differentials (ΔT_{BP}) were calculated by subtracting baseline temperatures (T_{Room}) from observed peak temperatures (T_{Peak}) for each supplied lamp energy density, and the resulting data are shown in Figure 2. The same pattern as that shown in Table 1 is observed.

2.3. Thermal Conductivity. The thermal conductivity for both BP and a known IX standard was calculated as described in the Methods section, as shown in Figure 3. The heat flow

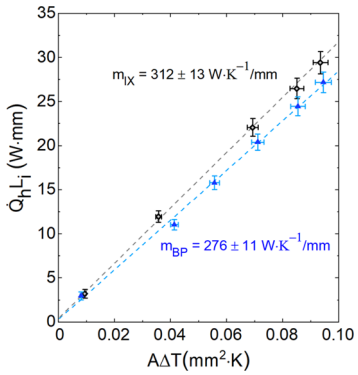

Figure 3. Thermal conductivity of BP and IX modeled using the York method for least-squares fitting.

approximation $\dot{Q}_h \propto \dot{Q}_i$ that was used in these calculations was validated by the linear response of the plots for both materials. Linear fitting was performed using the York method for least-squares fitting designed for data with quantified errors in both the x- and y-axes.[23]

Using the York method, the slopes were found to be m_{BP} = 276 ± 11 W/(K·mm) and m_{IX} = 312 ± 13 W/(K·mm). This resulted in a thermal conductivity value for BP sample k_{BP} = 10.6 ± 0.6 W/(m·K), calculated using the Origin Simple Linear Regression Model equation [$y = mx + b + \text{error}_{ms}$], where the error_{ms} is the mean-square error, and eq 2. Use of a linear regression model that does not account for the x and y errors in the fitting ($y = mx + b$) yielded k_{BP} = 10.7 ± 0.2 W/m·K. While this method underestimates the true uncertainty, it provides a simple check against systematic fitting errors due to the use of error bars in the York method. As the values of k given by the two models match closely, we take k_{BP} = 10.6 ± 0.6 W/(m·K) as our estimation of thermal conductivity.

3. DISCUSSION

The primary goal of the present work was to investigate the underlying thermal processes behind PTD by measuring the temperatures produced from irradiating BP sorbents with pulses of light, as well as the material's thermal conductivity. By quantifying these properties, the required energy density to produce the desired BP temperature could be estimated, so we were able to gain more insight into which VOC analytes would be ideal candidates for sampling and analysis using this method based on boiling point. With this goal in mind, research was conducted to determine the best method for measuring BP temperature changes in response to lamp energies at varying intensities. Both infrared (IR) cameras and thermocouples were initially considered as means of measuring BP thermal response. However, IR cameras typically only measure surface temperatures, while T/Cs allowed for internal material measurements via embedding. In addition, a study conducted by Michalski et al. revealed that surface temperature measurements conducted by IR camera and k-type T/C yielded similar data at 300 °C.[24] Michalski et al. also note that IR camera measurement uncertainty is dependent upon parameters such as camera distance, observation angle, and source interferences such as heating elements or lamps lighting the surface.[24] Considering PTD utilizes a xenon flash lamp as its heat source, and the general setup makes obtaining optimal observation angles difficult, if not impossible, the present work opted for the use of k-type T/Cs for quantifying thermal response.

Based on the data presented in Figure 2, the method of embedding thermocouples into BPs showed the highest recorded peak temperature changes during BP irradiation. In addition, the percent of lamp input temperature (T_I) measured as output temperature from the BPs (T_O), seen in Table 2, demonstrates that embedded BPs also measure the lowest conductive heat loss ($\%T_O/T_I$) with 74−86% of the incident temperature being conducted to the embedded T/C, as compared to the combined 48−71% conduction measured in pressed and adhered BPs (Table 2).

Though the present work has identified the best of the described methods for measuring BP temperature, the study also uncovered that the highest BP peak temperature measured was only 76 ± 4 °C and therefore was much lower than the

https://dx.doi.org/10.1021/acsomega.0c05613
ACS Omega 2021, 6, 5415−5422

Table 2. Percent Input Lamp Energy (T_I) Conducted through BP and Measured as Output Temperature (T_O)

energy density (J/cm^2)[b]	lamp temperature (°C)[a,c]	$\%T_O/T_I$[a,d]		
		P-BP	A−BP	EM-BP
0.28 ± 0.02	40.9 ± 1.1	71 ± 3	71 ± 3	86 ± 3
0.42 ± 0.01	48.9 ± 0.8	66 ± 5	67 ± 2	84 ± 2
0.728 ± 0.009	67.3 ± 0.6	56 ± 4	59 ± 3	79 ± 2
1.33 ± 0.01	102.8 ± 2.6	48 ± 5	54 ± 3	74 ± 4

[a]Values are depicted as mean ± standard deviation. [b]n = 30. [c]n = 3. [d]n = 9.

boiling points of many potential PTD compatible analytes. This caused a shift from the hypothesized means of picking desorption temperatures by analyte boiling point. However, considering that previous PTD studies by Floyd et al. demonstrated successful desorption of toluene over a range of energy densities[8] (T_{boil} = 110.7 °C),[25] it becomes evident that the input heat energy generated by PTD is sufficiently high to overcome the van der Waals forces holding analytes onto BP surfaces at temperatures below the analyte's boiling point, which means that PTD compatible analytes can be chosen based on the ability to be desorbed at the range of BP temperatures generated during PTD (i.e., 35.2−76 °C). It is worth noting that during data collection for BP temperature response, potential instrument limitations may have arisen. Though T/Cs were the most convenient measurement method for the study's needs, they are only capable of making point measurements as opposed to full-field measurements. This could cause an error in the data, as temperatures may differ across the BP surface due to its nonhomogeneous structure. Additionally, T/C response time (0.15 s)[26] was comparatively lower than the flash period of the lamp (0.0005 s).[22] This relatively slow response time could have potentially resulted in underestimated peak temperature measurements, possibly playing a contributing role in the observed 14−26% of heat loss observed in the $\%T_O/T_I$ calculations presented in Table 2. Any remaining discrepancies between T_O and T_I, particularly those observed for embedded BPs, may be attributed to potential limiting factors arising from the material morphology (Figure 1). These limiting factors may include the random alignment of the SWNT in our BPs, creating air-filled pores that may act as heat sinks, and/or the nonuniform dispersal of SWNTs during fabrication, leading to variability in the thickness of BP samples, which potentially allows for more heat to diffuse into the material than expected prior to reaching the T/C.

Having established the method for determining BP temperature change due to PTD, the study's experimental focus shifted to determining BP thermal conductivity as a means of obtaining a better understanding of how input energy is distributed throughout the sorbent body. Additionally, this metric will provide necessary insights on desorption and sorbent quality assurance, as sorbents with greater thermal conductivity are expected to desorb more evenly and withstand higher energy density exposures. For the purposes of this study, a comparative method was chosen to measure thermal conductivity. This was decided based upon the readily available instrumentation. While searching for an appropriately comparable, standardized reference material, attempts were made using materials with higher (copper and aluminum) or lower (acrylic) thermal conductivity values than IX. This resulted in derived k_{BP} values far from typical values for buckypaper, and roughly an order of magnitude different than the standard used. In the case where parasitic heat loss in a system is negligible one could apply linear fits as per eq 2 using any standardized reference, but in our case, the heat loss is non-negligible and will scale with the thermal conductivity of the standard. While this constraint requires that the standard be close in value to the material in question, it also provides a consistency check on our estimate of k_{BP}: $k_{BP} \approx k_{standard}$, or in our case, $k_{BP} \approx k_{IX}$. The largest source of error in this estimate is a determination of the heat flow through the sample, as heat losses can occur through air convection, radiation, or conduction through the solid apparatus and thermistor wires. While radiation loss can be minimized somewhat by working at close to room temperature, parasitic conduction losses are challenging to hold negligible. In addition, while we can remove convection losses via measurement in vacuum, the measurement was performed in air to obtain a practically useful value of k in porous BPs. Based on the collected thermal conductivity data, we note that no significant variance in k was observed in the initial and secondary measurements of the same BP strip or IX samples, nor of a second BP strip cut to the same dimensions and measured twice. Slight systematic errors may exist due to the small mismatch between k_{BP} and k_{IX}, but considering that the difference in k_{BP} and k_{IX} falls within 10%, this potential limitation likely only results in a small underestimation of Q_{loss}, which would create systematic error much smaller than our estimated uncertainty.[27] The value of k_{bp} found here is similar to the values reported in the literature for other BPs (10.5−12 W/(m·K)) measured under similar thermal conditions.[10,28,29]

4. CONCLUSIONS

In the present work, we have concluded that when irradiated with light pulses, similar with those used in PTD, BPs undergo a temperature increase of 11.2 ± 0.3 to 57.1 ± 0.6 °C based on measurements collected by an embedded thermocouple at room temperature, indicating 32.5 ± 0.9 to 76 ± 4 °C to be the range of desorption temperatures possible with the present PTD setup. Additionally, a linear regression model of BP thermal conductivity based on the steady-state comparative method revealed that arc discharge BPs have a thermal conductivity of 10.6 ± 0.6 W/(m·K), providing information on heat distribution and, in turn, the desorption capabilities across the sorbent body. We believe that this data provides a better understanding of the thermal properties behind the photothermal desorption technique's theoretical framework, specifically, the energy density necessary to attain a desired BP temperature and how that energy is distributed throughout the BP. These findings will prove to be vital steps toward understanding this developing analytical method.

5. METHODS

5.1. Buckypaper Fabrication. Presuspended (1 g/L solution of 1% w/v sodium cholate or sodium dodecyl sulfate in water) AD SWNTs (94.5% pure, 1.2−1.7 nm diameter, 0.1−4 μm length) were obtained from Nanointegris Inc. (Quebec, Canada) and used to fabricate self-supporting BPs. In accordance with the manufacturers' suggestions and our previous works,[16,17,30] 50 mL of AD SWNT solution was mixed with 400 mL of acetone (ACS grade) for 15 h. The solution was vacuum-filtered against a poly-

https://dx.doi.org/10.1021/acsomega.0c05613
ACS Omega 2021, 6, 5415−5422

(tetrafluoroethylene) (PTFE) membrane filter (47 mm diameter, 5 μm pore size, EMD Milipore, Darmstadt, Germany), allowing for 30 min of vacuum drying after filtration, and subsequently subjected to two, two-step cleaning cycles consisting of a rinse with 250 mL of HPLC grade water and a rinse with 40 mL of acetone. The SWNT cake was then allowed to vacuum-dry for 30 min, followed by an additional 2 h of air drying, ultimately producing a self-supporting BP that was delaminated from the PTFE membrane.

Similar to our previous reports,[17,30] BPs were heat-treated using a muffle furnace (Thermolyne F48025-60-80, Thermo Fisher Scientific, Waltham, MA) to remove residual solvents and surfactants remaining from fabrication. Samples were heated to 300 °C at a ramping rate of 10 °C/min and held at temperature for 90 min, before cooling back to room temperature (~24 °C). The BPs were then placed into 100 °C storage. The morphology of the heat-treated BPs was examined using a scanning electron microscope (Tescan Lyra FIB-FESEM, Kohoutovice, Czech Republic).

5.2. Thermocouple Attachment. Fast response (0.15 s), cement-on thermocouples (T/C; k-type; chrome (+); alumel (−); foil thickness 0.0005″) were purchased from Omega Engineering Inc.[26] (Norwalk, CT) and modified slightly by trimming away the excess polyimide film surrounding the T/C leads (Figure 4a,b). Trimming was performed in a zigzag pattern (Figure 4b) to provide more surface for SWNTs to weave around during fabrication, thus creating a more secure hold on the T/C. Embedded BP fabrication followed the procedure outlined in the previous section, with the embedding of T/Cs taking place during the vacuum filtration of suspended SWNTs. A T/C was introduced into the SWNTs suspended above the membrane once approximately one-third of the supernatant liquid had been filtered, allowing the T/C to be embedded between the laminated and still-suspended nanotubes.

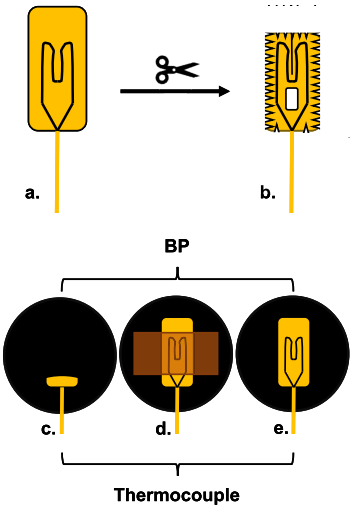

Figure 4. (a) As-received T/C lead; (b) trimmed lead. (c−e) Three thermocouple attachment methods: embedding (c), adhering via a polyimide tape (d), and pressing (e). (c) Top-down view of a BP, while (d) and (e) represent a bottom-up view.

In addition to embedding (Figure 4c), nonmodified T/Cs were also mounted to BPs by pressing and adhesion. Pressed BPs were seated on the surface of the T/C and pressed into place by a glass cover (Figure 4e). Adhered BPs followed a similar setup but were also secured to the T/C by a polyimide tape (i.e., adhered; 2.54 cm × 1.27 cm strip), as seen in Figure 4d.

5.3. Light Energy and Thermal Response. A photographic grade, xenon flash lamp (Neewer 300 W, Neewer Technology, Shenzhen Guangdong, China) was used as the PTD light source (Figure 5a). To determine the range of energy densities produced by the lamp, a Nova II laser power and energy meter (Ophir-Spiricon, LLC., North Logan, Utah) was pulsed 30 times over four lamp settings (i.e., 3.0, 4.0, 5.0, 6.0), and the four corresponding energy densities (0.28, 0.42, 0.728, and 1.33 J/cm^2) were used to determine the thermal response of BPs. The PTD system was setup as seen in Figure 5a, with a T/C installed inside a 5.75 cm^3 aluminum chamber (Figure 5b); the system was then closed by securing a glass plate over the chamber using a screw-on, metal top ring (Figure 5b). Each BP (n = 3 for all mounting methods) was placed under a N_2 (g) flow (Q = 0.5 L/min) and exposed in triplicate to the four energy densities produced by the xenon flash lamp (t_{flash} = 0.0005 s)[22] positioned 2.9 ± 0.2 mm (n = 5) above the sample. The resulting data points were logged using a data acquisition chassis with mini T/C input (DAQ; National Instruments; Austin, TX) and analyzed using DAQExpress software (version 3.0.0; National Instruments; Austin, TX).

A multiple linear regression model was fitted for testing if the peak BP thermal responses, measured using the three different T/C mounting methods (i.e., pressing, adhering, and embedding), were the same. Considering the high correlation between lamp setting and the peak temperature, the lamp setting was adjusted in the regression model. Tukey's test[31] was used when testing the thermal responses pairwise. The goodness of fit of the regression model was assessed using R-squared values.

5.4. Thermal Conductivity. The thermal conductivity of an AD BP was determined using the steady-state comparative technique shown in Figure 6, wherein a thin strip of a BP is laid in firm thermal contact via conductive silver paint between a positive temperature coefficient (PTC) aluminum heater and a copper heat sink in thermal equilibrium with the room, with two isolated thermistors placed 10 mm apart in the intervening space and in thermal contact with the laid strip. This method utilizes Fourier's law of heat conduction

$$k = \frac{\dot{Q}_i L}{A\Delta T} \tag{1}$$

where $\dot{Q}_i$ is the rate of heat flow (J) through the strip of material i, A is the cross-sectional area of the strip (m^2; width w × thickness t), ΔT is the temperature difference (K) between the intermediary thermistors, and L is the distance (m) between the thermistors.[32] Replicate measurements (n = 4) were performed in air to obtain a practically useful and reproducible value of k in porous BPs.

Our comparative technique using Fourier's law assumed equal heat flow and equal losses between two measurements. This approximation is accurate if the sample of interest and the known reference have physical dimensions, thermal contact resistances and areas, and thermal conductivities that are as similar as possible. A strip of Inconel X-750 (IX; k_{IX} = 11.96 W/(m·K)) cut to identical dimensions as the BP (3.18 mm wide, 0.11 mm thick, 30 mm long) was selected as a reference, based on previous reports of similarly made BPs in which

https://dx.doi.org/10.1021/acsomega.0c05613
ACS Omega 2021, 6, 5415−5422

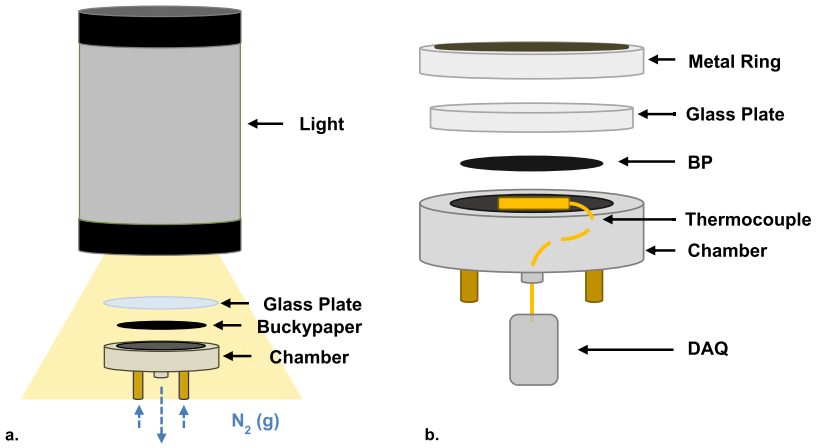

Figure 5. (a) General PTD setup; (b) general T/C setup within the PTD chamber.

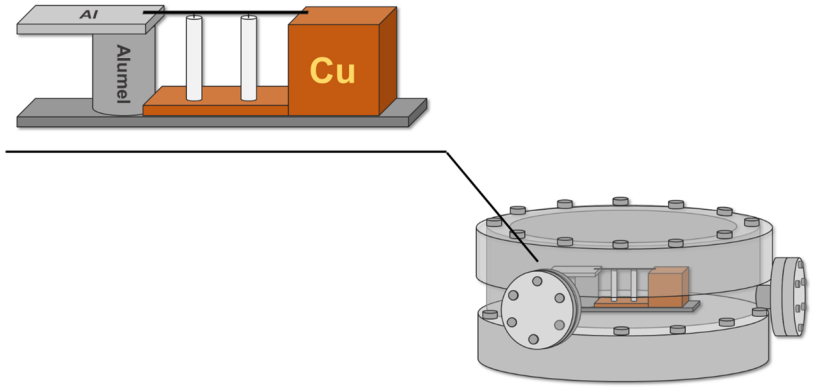

Figure 6. Steady-state comparative technique for quantifying thermal conductivity—(Top left) BP strip sits across a PTC aluminum heater, thermistors, and a copper heat sink; (bottom right) a vacuum chamber used to house the measurement device.

thermal conductivity of ~10 W/(m·K)[10,28,29] was reported. IX is also an excellent choice due to its low variation in thermal conductivity (±5% above 100 K)[33] in our experimental temperature range.

Within our small experimental temperature range (290−315 K), we assumed that the parasitic heat loss $\dot{Q}_{loss} = \dot{Q}_h - \dot{Q}_i$ would scale linearly with heater power $\dot{Q}_h$. Previous measurements of bulk single-wall nanotubes and IX show similar percentage linear increases in thermal conductivity with temperature, supporting a general approximation of $\dot{Q}_h \propto \dot{Q}_i$.[27,34] By applying eq 1 for both IX and BP, within these constraints, the thermal conductivity of the BP is given by

$$k_{BP} = k_{IX} \frac{\frac{\dot{Q}_{BP} L_{BP}}{A_{BP}\Delta T_{BP}}}{\frac{\dot{Q}_{IX} L_{IX}}{A_{IX}\Delta T_{IX}}} = k_{IX} \frac{m_{BP}}{m_{IX}} \quad (2)$$

where m_i is the linear fit slope of the graph of $\dot{Q}_i L_i$ as a function of $A_i \Delta T_i$, created by measuring the same sample at a series of heater powers without change to the surrounding environment and without moving or changing the material strip in question. In the regime where $\dot{Q}_h \propto \dot{Q}_i$, m is linear and provides a check to the assumption conditions.

■ ASSOCIATED CONTENT

Supporting Information

The Supporting Information is available free of charge at https://pubs.acs.org/doi/10.1021/acsomega.0c05613.

Standard arc discharge single-walled carbon nanotube buckypaper, a trimmed k-type thermocouple, and a trimmed thermocouple embedded within a buckypaper (Figure S1); general PTD setup with a flash lamp and a PTD setup with a desorption chamber (Figure S2); experimental setup for quantifying BP thermal conductivity; an additional Buckypaper SEM imageryheater, thermistors, and a copper heat sink (Figure S3) (PDF)

■ AUTHOR INFORMATION

Corresponding Author

Claudiu T. Lungu − *Department of Environmental Health Sciences, University of Alabama at Birmingham, Birmingham, Alabama 35233, United States;* orcid.org/0000-0001-8777-1649; Email: clungu@uab.edu

Authors

Jacob S. Shedd − *Department of Environmental Health Sciences, University of Alabama at Birmingham, Birmingham, Alabama 35233, United States;* orcid.org/0000-0003-4780-3399

Wyatt W. Kuehster − *Department of Physics & Astronomy, University of Alabama, Tuscaloosa, Alabama 35487, United States*

Smriti Ranjit − *Department of Physics & Astronomy, University of Alabama, Tuscaloosa, Alabama 35487, United States*

https://dx.doi.org/10.1021/acsomega.0c05613
ACS Omega 2021, 6, 5415−5422

Adam J. Hauser − *Department of Physics & Astronomy, University of Alabama, Tuscaloosa, Alabama 35487, United States*
Evan L. Floyd − *Department of Occupational and Environmental Health, University of Oklahoma, Oklahoma 73104, United States*
Jonghwa Oh − *Department of Environmental Health Sciences, University of Alabama at Birmingham, Birmingham, Alabama 35233, United States*

Complete contact information is available at: https://pubs.acs.org/10.1021/acsomega.0c05613

Author Contributions

The manuscript was written through the contributions of all authors. All authors have given approval to the final version of the manuscript.

Notes

The authors declare no competing financial interest.

■ ACKNOWLEDGMENTS

This study was supported by The Deep South Center for Occupational Health and Safety (Grant #5T42OH008436-15 from the National Institute of Occupational Safety and Health, NIOSH). Its contents are solely the responsibility of the authors and do not necessarily represent the official views of NIOSH. Additional acknowledgments go to Boyi Guo, from the Department of Biostatistics at the University of Alabama at Birmingham, for contributing his time and statistical knowledge toward modeling the BP thermal response data.

■ ABBREVIATIONS

VOC, volatile organic compound; PTD, photothermal desorption; BP, buckypaper; T/C, thermocouple; CD, chemical desorption; SWNTs, single-walled carbon nanotubes; AD, arc discharge; PTFE, poly(tetrafluoroethylene); PTC, positive temperature coefficient; IX, Inconel X-750

■ REFERENCES

(1) U. S. Bureau of Labor Statistics. May 2017 National Occupational Employment and Wage Estimates United States. https://www.bls.gov/oes/2017/may/oes_nat.htm (accessed 2019-04-02).
(2) *Hydrocarbons, BP 36°-216 °C (NIOSH-1500), NIOSH Manual of Analytical Methods*; NIOSH, 1994; Vol. *2*, pp 811.
(3) *Hydrocarbons, Aromatic (NIOSH-1501), NIOSH Manual of Analytical Methods*; NIOSH, 2003; Vol. *127*, 3, pp 17.
(4) Carl, J.; Elskamp, O. S. H. A. Sampling and Analytical Methods—Toluene (Organic Method #111). https://www.osha.gov/dts/sltc/methods/organic/org111/org111.pdf (accessed 2020-12-22).
(5) Occupational Safety and Health Administration. 29 CFR 1910. https://www.osha.gov/laws-regs/regulations/standardnumber/1910 (accessed 2020-12-22).
(6) National Institute for Occupational Safety and Health (NIOSH). NIOSH Pocket Guide to Chemical Hazards. https://www.cdc.gov/niosh/npg/default.html (accessed 2020-12-22).
(7) *2019 TLVs and BEIs*, American Conference of Governmental Industrial Hygienists (ACGIH); ACGIH Signature Publications: Cincinnati, 2019.
(8) Floyd, E. L.; Sapag, K.; Oh, J.; Lungu, C. T. Photothermal Desorption of Single-Walled Carbon Nanotubes and Coconut Shell-Activated Carbons Using a Continuous Light Source for Application in Air Sampling. *Ann. Occup. Hyg.* **2014**, *58*, 877−888.
(9) Oh, J. Fabrication and Characterization of Buckypapers for Use in Air Sampling. Ph.D. Dissertation, University of Alabama at Birmingham, 2016.
(10) Kumanek, B.; Janas, D. Thermal Conductivity of Carbon Nanotube Networks: A Review. *J. Mater. Sci.* **2019**, *54*, 7397−7427.
(11) Mishra, L. P.; Mishra, L. K. A Theoretical Evaluation of Temperature Dependent Thermal Conductivity of Carbon Nanotube. *Int. J. Chem. Sci.* **2015**, *13*, 672−682.
(12) Mizuno, K.; Ishii, J.; Kishida, H.; Hayamizu, Y.; Yasuda, S.; Futaba, D. N.; Yumura, M.; Hata, K. A Black Body Absorber from Vertically Aligned Single-Walled Carbon Nanotubes. *Proc. Natl. Acad. Sci. U.S.A.* **2009**, *106*, 6044−6047.
(13) Sysoev, N. N.; Osipov, A. I.; Uvarov, A. V.; Kosichkin, O. A. Flash Ignition of a Carbon Nanotube. *Moscow Univ. Phys. Bull.* **2011**, *66*, 492−494.
(14) Feng, Y.; Inoue, T.; An, H.; Xiang, R.; Chiashi, S.; Maruyama, S. Quantitative Study of Bundle Size Effect on Thermal Conductivity of Single-Walled Carbon Nanotubes. *Appl. Phys. Lett.* **2018**, *112*, No. 191904.
(15) Floyd, E. L. Photothermal Deorption of Toluene From Single Walled Carbon Nanotubes and Activated Carbon Sorbents. Ph.D. Dissertation, University of Alabama at Birmingham, 2013.
(16) Oh, J.; Floyd, E. L.; Watson, T. C.; Lungu, C. T. Fabrication and Adsorption Characterization of Single-Walled Carbon Nanotubes (SWNT) Buckypaper (BP) for Use in Air Samples. *Anal. Methods* **2016**, *8*, 4197−4203.
(17) Oh, J.; Floyd, E. L.; Parit, M.; Davis, V. A.; Lungu, C. T. Heat Treatment of Buckypaper for Use in Volatile Organic Compounds Sampling. *J. Nanomater.* **2016**, *2016*, No. 3248059.
(18) Misra, P.; Casimir, D.; Craig, C.; Garcia-sanchez, R.; Baliga, S. Thermal Characterization of Single-Walled Carbon Nanotubes and Tungsten Oxide-Based Nanomaterials via Raman Spectroscopy. In *Recent Trends in Materials and Devices*; Springer: Cham, 2017; Vol. *178*, pp 3−8.
(19) Balandin, A. A.; Ghosh, S.; Bao, W.; Calizo, I.; Teweldebrhan, D.; Miao, F.; Lau, C. N. Superior Thermal Conductivity of Single-Layer Graphene. *Nano Lett.* **2008**, *8*, 902−907.
(20) Li, Q.; Liu, C.; Wang, X.; Fan, S. Measuring the Thermal Conductivity of Individual Carbon Nanotubes by the Raman Shift Method. *Nanotechnology* **2009**, *20*, No. 145702.
(21) Li, M.; Yue, Y. Raman-Based Steady-State Thermal Characterization of Multiwalled Carbon Nanotube and Buckypaper.Pdf. *J. Nanaosci. Nanotechnol.* **2015**, *15*, 3004−3010.
(22) Neewer 600 W(2-Pack 300W)5600 K Photo Studio Strobe Flash Light Monolight with Modeling Lamp, Aluminium Alloy Speedlite for Indoor Studio Location Model Photography, Portrait Photography(N-300W). https://support.neewer.com/product/neewer-600w2-pack-300w5600k-photo-studio-strobe-flash-light-monolight-with-modeling-lampaluminium-alloy-speedlite-for-indoor-studio-location-model-photographyportrait-photographyn-300w/ (accessed 2020-08-06).
(23) York, D.; Evensen, N. M.; López Martinez, M.; Delgado, J. D. B. Unified Equations for the Slope, Intercept, and Standard Errors of the Best Straight Line. *Am. J. Phys.* **2004**, *72*, 367−375.
(24) Michalski, D.; Strak, K.; Piasecka, M. Comparison of Two Surface Temperature Measurement Using Thermocouples and Infrared Camera. *EPJ Web Conf.* **2017**, *143*, No. 02075.
(25) National Institute of Standards and Technology. NIST Chemistry WebBook, SRD 69: Toluene. https://webbook.nist.gov/cgi/cbook.cgi?ID=C108883&Mask=4#Thermo-Phase (accessed 2020-11-05).
(26) Omega. "Cement-On" Thermocouples. https://assets.omega.com/spec/CO-K.pdf (accessed 202008-06).
(27) Hone, J.; Whitney, M.; Piskoti, C.; Zettl, A. Thermal Conductivity of Single-Walled Carbon Nanotubes. *Phys. Rev. B* **1999**, *59*, 2514−2516.
(28) Yang, K.; He, J.; Puneet, P.; Su, Z.; Skove, M. J. Tuning Electrical and Thermal Connectivity in Multiwalled Carbon Nanotube Buckypaper. *J. Phys.: Condens. Matter* **2010**, *22*, No. 334215.

(29) Gonnet, P.; Liang, Z.; Choi, E. S.; Kadambala, R. S.; Zhang, C.; Brooks, J. S.; Wang, B.; Kramer, L. Thermal Conductivity of Magnetically Aligned Carbon Nanotube Buckypapers and Nanocomposites Q. *Curr. Appl. Phys.* **2006**, *6*, 119−122.
(30) Shedd, J. S.; Floyd, E. L.; Oh, J.; Lungu, C. T. FTIR Determination of Surfactant Removal from Arc Discharge Buckypapers for Air Sampling. *J. Adv. Nanomater.* **2019**, *4*, 11−16.
(31) Tukey, J. Comparing Individual Means in the Analysis of Variance. *Biometrics* **1949**, *5*, 99−114.
(32) Fourier, J. Theorie Analytique de La Chaleur, 1822, F. Didot, Paris, Republication of English Translation That First Appeared in 1878. In *The Analytical Theory of Heat*; The University Press, 1955.
(33) Pawel, R. E.; Williams, R. K. *Survey of Physical Property Data for Several Alloys*, No. ORNL/TM--9616; Oak Ridge National Lab: 1985.
(34) Special Metals Corporation. Inconel Alloy X-750. https://www.specialmetals.com/assets/smc/documents/alloys/inconel/inconel-alloy-x-750.pdf (accessed 2020-07-06).

https://dx.doi.org/10.1021/acsomega.0c05613
ACS Omega 2021, 6, 5415−5422